International Journal of Pressure Vessels and Piping 201 (2023) 104872

Contents lists available at ScienceDirect

International Journal of Pressure Vessels and Piping

journal homepage: www.elsevier.com/locate/ijpvp

Optimization design on resonance avoidance for 3D piping systems based on wave approach

Xiangliang Wang, Pingzhang Zhou, Yun Ma *, Gengkai Hu **

School of Aerospace Engineering, Beijing Institute of Technology, Beijing, 100081, China

ARTICLE INFO

Keywords:
Wave approach
Genetic algorithm
3D piping system
Shape optimization
Rigid hanger location

ABSTRACT

Vibration of liquid conveying piping systems in a closure may cause noising problem and degrade living comfort inside, it can even lead to fatigue failure of the system. Therefore, vibration alleviation in such circumstance is highly demanded. Traditionally, a piping system is designed to satisfy basic key functions as liquid conveying or heat exchange. Once the global arrangement of a piping system is determined for such key functions, local modifications with hangers on the piping system are then made to reduce its vibration. Here, we propose a method to optimize globally the shape and rigid hanger locations for a 3D piping system in order to achieve resonance avoidance. To this end, the wave approach is employed to estimate in a fast and accurate way the fundamental frequency of any 3D liquid conveying piping system, assembled from some basic elements. Based on genetic algorithm, optimization on shape and rigid hanger locations for a 3D piping system can be obtained with a maximal fundamental frequency, which is far away from the external excitation frequency. It shows that the shape optimization can be used to increase the fundamental frequency of a piping system if rigid hangers are not available, while the fundamental frequency can be increased more effectively with rigid hangers of optimized locations. Our work provides a systematic method for global optimization design of 3D piping systems.

1. Introduction

Fluid conveying piping systems are widely used in modern transportation equipment such as ships, aircraft, automobile, just to name a few [1–3]. A liquid-filled piping system will be subjected to obvious vibrations induced by different kinds of external and internal loads during its function [4], radiating uncomfortable noise which should be largely reduced when designing ship or aircraft cabins [5,6]. The present design methodology of a piping system is usually as following: the layout of the pipeline is firstly determined by key functions such as liquid conveying or heat exchange, then local arrangement of the pipe section with high vibration amplitude is improved by imposing constraints [7]. Studies on the vibration optimization of an entire pre-designed piping system are few.

There are analytical solutions for calculating vibration response of a pipe with simple geometry such as a cantilevered straight pipe, but for a complex 3D piping system, finite element method (FEM) [8–10] or wave approach [11,12] (also called spectral element method (SEM) [13–15]) have to be employed for its vibration analysis. Compared to FEM, the wave approach is more efficient. In addition, the computational accuracy of FEM is highly affected by its element size; while, wave approach as an approximate analytical method, is free from the element size and has higher computational efficiency when solving a complex 3D piping system. In the recent years, the large-amplitude vibrations of pipes conveying fluid were also explored by several researchers, by using, for example, geometrically exact model [16,17] and absolute nodal coordinate formulation [18–22].

In general, optimization of a piping system includes its layout optimization as well as vibration control (i.e., resonance avoidance). For the layout optimization, the ship or aero-engine pipe route design can be carried out by using genetic algorithm [7,23,24], cooperative coevolution [24], concurrent ant colony optimization algorithm [25] and modified particle swarm optimization [26,27]. In all above studies, when optimizing the route of the piping system, the vibrational characteristics of the piping system is not taken into account, which however cannot be neglected in studying 3D piping systems optimization.

For the vibration control, firstly, the pipe supports (i.e. hoops, rigid hangers or clamps) were utilized to reduce vibration of the 3D piping

* Corresponding author.
** Corresponding author.
E-mail addresses: yun_ma@bit.edu.cn (Y. Ma), hugeng@bit.edu.cn (G. Hu).

https://doi.org/10.1016/j.ijpvp.2022.104872
Received 28 October 2022; Received in revised form 9 December 2022; Accepted 20 December 2022
Available online 21 December 2022

system through optimizing their positions [28]. Tang et al. [29] optimized the hoop positions to reduce the maximal stress and strain of a 3D piping system, and Zhang et al. [30,31] used non-probabilistic sensitivity analysis to eliminate insensitive hoops. Kwong and Edge [32] carried out an investigation on the location optimization of the pipe clamps mounted on a flexible frame, so as to minimize the force exerted by the pipe on the flexible frame. Through numerical simulation, Liu et al. optimized further the local layout of hoops for reducing vibration amplitude as well as for avoiding resonance based on the particle swarm algorithm [33] and genetic algorithm [34], respectively. Secondly, the periodic support system can be regarded as effective filters to control the vibration of piping systems [35]. Mead [36] studied the effect of wave propagation constant for a periodically supported infinite beam. In detail, wave approach was utilized by Koo and Park [37] to investigate wave bandgaps for a 3D piping system, they found that a proper design of periodic supports for reducing vibration in a specific frequency range is possible. In addition, Yu et al. [38–44] investigated wave bandgaps of periodic pipe systems based on phononic crystal theory, and found that the low frequency band gaps can provide a new method for vibration control. Wu et al. designed periodic dynamic vibration absorbers (DVAs) attached on a pipe to reduce its vibration [45], and also proposed a periodically supported pipe–plate model to analyse the effect of an elastic plate on vibration bandgap [46].

Design and optimization of piping systems aim to avoid resonance, leading FF to be higher than excitation frequency [34,47]. Thus, in order to find a solution in a faster and efficient way for achieving global resonance avoidance of a 3D piping system, the following three aspects should be further considered: one is to include the effect of fluid flow on vibration of piping systems with wave approach; the second is that shape (route) optimization for avoiding resonance should be considered; the last is to extend the optimization of hanger location from a pipe segment to the whole 3D piping system. These are main objectives of this manuscript. Consequently, we will carry out a study on the resonance avoidance of a 3D piping system through optimizing its pipe shape and rigid hanger location using wave approach. The manuscript will be organized as follows. In Section 2, we develop a 3D model for vibration analysis of a piping system with wave approach, and its efficiency is demonstrated. In Section 3, a typical 3D piping system is selected and its dynamic characteristics with/without fluid flow are discussed. In Section 4, the numerical examples of shape and rigid hanger location optimization of a 3D piping system are provided to illustrate the developed optimization method. Finally, a brief summary of the conclusions is outlined in Section 5.

2. Methods

2.1. Wave approach for vibration analysis

2.1.1. Vibration governing equations

Generally, a 3D liquid-conveying piping system can be divided into straight pipe segments and curved ones. The dynamic stiffness matrices of the straight and curved pipe elements will be calculated separately, and then assembled to form the global dynamic stiffness matrix of the entire 3D piping system. As illustrated in Fig. 1, the straight pipe element has 2 nodes, and there are 6° of freedom at each node, in which y_L, y_R, z_L, z_R, u_L and u_R represent the nodal displacements and θ_{yL}, θ_{yR}, θ_{zL}, θ_{zR}, φ_L, φ_R the nodal rotations of left and right ends, respectively, and C represents the fluid velocity. The governing equations of a straight pipe element have been derived by Koo and Park [11], in which the vibration motion of a differential element of the pipe can be expressed by four parts:

$$E(1+j\alpha)I\frac{\partial^4}{\partial x^4}y(x,t)+pA_f\frac{\partial^2}{\partial x^2}y(x,t)+\rho_pA_p\frac{\partial^2}{\partial t^2}y(x,t)=F_{ye}(x,t)+F_{yf}(x,t), \tag{1}$$

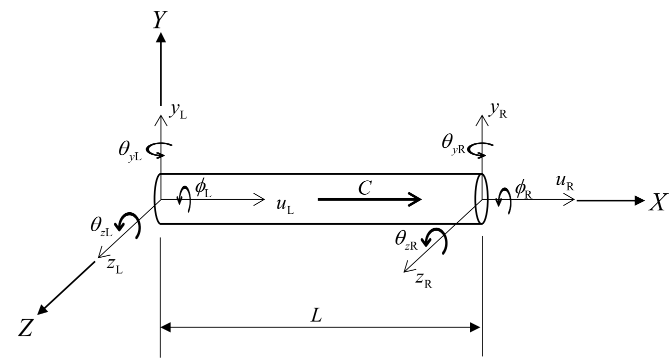

Fig. 1. Straight pipe element. Flexural vibration in (*x, y*)-plane.

flexural vibration in (*x, z*)-plane:

$$E(1+j\alpha)I\frac{\partial^4}{\partial x^4}z(x,t)+pA_f\frac{\partial^2}{\partial x^2}z(x,t)+\rho_pA_p\frac{\partial^2}{\partial t^2}z(x,t)=F_{ze}(x,t)+F_{zf}(x,t), \tag{2}$$

torsional vibration:

$$J\frac{\partial^2}{\partial t^2}\varphi(x,t)-G(1+j\beta)I_p\frac{\partial^2}{\partial x^2}\varphi(x,t)=M_{te}(x,t), \tag{3}$$

axial vibration:

$$\rho_pA_p\frac{\partial^2}{\partial t^2}u(x,t)-E(1+j\alpha)A_p\frac{\partial^2}{\partial x^2}u(x,t)=P_e(x,t)+P_f(x,t), \tag{4}$$

where E and G are Young's elastic modulus and elastic shear modulus, α and β are internal loss factors of the pipe material, I and I_p are moment and polar moment of inertia of pipe cross section, J is polar moment of inertia of pipe per unit length, p is internal pressure, ρ_p is the mass density and A_p is cross-sectional area of pipe. F_{ye} and F_{yf} are external mechanical force and fluid-dynamic force in y direction, F_{ze} and F_{zf} are those in z direction, M_{te}, P_e and P_f are the torque, axial external mechanical force and axial fluid-dynamic force. The subscripts e and f represent externally applied mechanical forces and inviscid fluid-dynamic forces, respectively.

In addition, one key factor influencing vibration motion of pipe is the speed of water flow, which can be idealized as inviscid flow. In steady condition, based on the theory of plug flow model, the inviscid fluid-dynamic forces acting on the pipe can be expressed as [3,48] flexural vibration in (*x, y*)-plane:

$$F_{yf}(x,t)=-\rho_fA_f\left[\frac{\partial^2}{\partial t^2}+2C\frac{\partial^2}{\partial x\partial t}+C^2\frac{\partial^2}{\partial x^2}\right]y(x,t), \tag{5}$$

flexural vibration in (*x, z*)-plane:

$$F_{zf}(x,t)=-\rho_fA_f\left[\frac{\partial^2}{\partial t^2}+2C\frac{\partial^2}{\partial x\partial t}+C^2\frac{\partial^2}{\partial x^2}\right]z(x,t), \tag{6}$$

axial vibration:

$$P_f(x,t)=-\rho_fA_f\frac{\partial^2}{\partial t^2}u(x,t), \tag{7}$$

where ρ_f is fluid density and A_f is cross-sectional area of fluid. The negative value means the reaction force applying on the pipe. The three terms in Equation (5) and Equation (6) represent inertial force, Coriolis force, and centrifugal force, respectively. Equation (7) represents the inertial force in axial direction.

For a harmonic excitation, the responses should have a harmonic part $e^{i\omega t}$. For examples, the flexural, torsional and axial vibration responses should be expressed as $Ye^{i\omega t}$ and $Ze^{i\omega t}$, $\Phi e^{i\omega t}$, and $Ue^{i\omega t}$, where Y,

Z, Φ and U are the corresponding amplitudes, and ω, i and t are circular frequency, imaginary unit and time, respectively. For a steady state vibration, harmonic part $e^{i\omega t}$ can be omitted.

After substituting Equations (5)–(7) into equations (1)–(4) and setting external forces on differential element of the pipe as zero, we can get in frequency domain the vibration Equations 8–11 as flexural vibration in (x, y)-plane:

$$E(1+j\alpha)I\frac{\partial^4}{\partial x^4}Y(x,\omega)+\left(\rho_f A_f C^2+pA_f\right)\frac{\partial^2}{\partial x^2}Y(x,\omega)+j2\rho_f A_f \omega C\frac{\partial}{\partial x}Y(x,\omega)-\left(\rho_p A_p+\rho_f A_f\right)\omega^2 Y(x,\omega)=0, \tag{8}$$

flexural vibration in (x, z)-plane:

$$E(1+j\alpha)I\frac{\partial^4}{\partial x^4}Z(x,\omega)+\left(\rho_f A_f C^2+pA_f\right)\frac{\partial^2}{\partial x^2}Z(x,\omega)+j2\rho_f A_f \omega C\frac{\partial}{\partial x}Z(x,\omega)-\left(\rho_p A_p+\rho_f A_f\right)\omega^2 Z(x,\omega)=0, \tag{9}$$

torsional vibration:

$$G(1+j\beta)I_p\frac{\partial^2}{\partial x^2}\Phi(x,\omega)+J\omega^2\Phi(x,\omega)=0, \tag{10}$$

axial vibration:

$$E(1+j\alpha)A_p\frac{\partial^2}{\partial x^2}U(x,\omega)+\left(\rho_p A_p+\rho_f A_f\right)\omega^2 U(x,\omega)=0. \tag{11}$$

2.1.2. Dynamic stiffness matrix of straight and curved pipe segments

The general solutions of Equations 8–11 should have the following forms:

$$\begin{aligned} &Y(x)=\sum_{n=1}^{4}A_{1n}e^{k_{an}x},\ \Theta_z=Y'(x)=\sum_{n=1}^{4}A_{1n}k_{an}e^{k_{an}x}\\ &Z(x)=\sum_{n=1}^{4}A_{2n}e^{k_{an}x},\ \Theta_y=-Z'(x)=-\sum_{n=1}^{4}A_{2n}k_{an}e^{k_{an}x},\\ &U(x)=\sum_{n=1}^{2}C_n e^{k_{cn}x},\ \Phi(x)=\sum_{n=1}^{2}B_n e^{k_{bn}x} \end{aligned} \tag{12}$$

where k_a, k_b, k_c are wave numbers, and A, B, C are coefficients to be determined. For a straight pipe element, the displacements of its two ends can be expressed by Equation (13) as flexural vibration in (x, y)-plane:

$$\begin{Bmatrix} Y_L\\ \Theta_{zL}\\ Y_R\\ \Theta_{zR}\end{Bmatrix}=\begin{bmatrix}1&1&1&1\\ k_{a1}&k_{a2}&k_{a3}&k_{a4}\\ e^{k_{a1}L}&e^{k_{a2}L}&e^{k_{a3}L}&e^{k_{a4}L}\\ k_{a1}e^{k_{a1}L}&k_{a2}e^{k_{a2}L}&k_{a3}e^{k_{a3}L}&k_{a4}e^{k_{a4}L}\end{bmatrix}\begin{Bmatrix}A_{11}\\ A_{12}\\ A_{13}\\ A_{14}\end{Bmatrix}, \tag{13a}$$

flexural vibration in (x, z)-plane:

$$\begin{Bmatrix} Z_L\\ \Theta_{yL}\\ Z_R\\ \Theta_{yR}\end{Bmatrix}=\begin{bmatrix}1&1&1&1\\ -k_{a1}&-k_{a2}&-k_{a3}&-k_{a4}\\ e^{k_{a1}L}&e^{k_{a2}L}&e^{k_{a3}L}&e^{k_{a4}L}\\ -k_{a1}e^{k_{a1}L}&-k_{a2}e^{k_{a2}L}&-k_{a3}e^{k_{a3}L}&-k_{a4}e^{k_{a4}L}\end{bmatrix}\begin{Bmatrix}A_{21}\\ A_{22}\\ A_{23}\\ A_{24}\end{Bmatrix}, \tag{13b}$$

torsional vibration:

$$\begin{Bmatrix}\Phi_L\\ \Phi_R\end{Bmatrix}=\begin{bmatrix}1&1\\ e^{k_{b1}L}&e^{k_{b2}L}\end{bmatrix}\begin{Bmatrix}B_1\\ B_2\end{Bmatrix}, \tag{13c}$$

axial vibration:

$$\begin{Bmatrix}U_L\\ U_R\end{Bmatrix}=\begin{bmatrix}1&1\\ e^{k_{c1}L}&e^{k_{c2}L}\end{bmatrix}\begin{Bmatrix}C_1\\ C_2\end{Bmatrix}. \tag{13d}$$

Equation (13) can be further expressed in a compact form as flexural vibration in (x, y)-plane:

$$[\mathbf{W_e}]_a=[\mathbf{D}_1]_a\mathbf{A}_a, \tag{14a}$$

flexural vibration in (x, z)-plane:

$$[\mathbf{W_e}]_b=[\mathbf{D}_1]_b\mathbf{A}_b, \tag{14b}$$

torsional vibration:

$$[\mathbf{W_e}]_c=[\mathbf{D}_1]_c\mathbf{A}_c, \tag{14c}$$

axial vibration:

$$[\mathbf{W_e}]_d=[\mathbf{D}_1]_d\mathbf{A}_d, \tag{14d}$$

where $\mathbf{A}$ and $\mathbf{W}_e$ represent the coefficient vector and displacement vector of a straight pipe element ends, and the subscripts (a, b, c, d) represent 4 vibration motions. According to Euler beam theory, when the length of the straight pipe element is larger than its diameter, the elastic restoring shear force, bending moments, torsional moment and axial force can be obtained respectively by flexural vibration in (x, y)-plane:

$$\begin{cases} S_y(x)=-E(1+j\alpha)IY'''(x)\\ M_z(x)=E(1+j\alpha)IY''(x)\end{cases}, \tag{15a}$$

flexural vibration in (x, z)-plane:

$$\begin{cases} S_z(x)=-E(1+j\alpha)IZ'''(x)\\ M_y(x)=-E(1+j\alpha)IZ''(x)\end{cases}, \tag{15b}$$

torsional vibration:

$$M_t(x)=G(1+j\beta)I_p\Phi'(x), \tag{15c}$$

axial vibration:

$$P(x)=E(1+j\alpha)A_pU'(x), \tag{15d}$$

where S_y and M_z are shear force and bending moment of the (x, y)-plane, S_z and M_y are shear force and bending moment of the (x, z)-plane, M_t is torsional moment, and P is tensile force.

The forces applied at both ends of the straight pipe element can be expressed as flexural vibration in (x, y)-plane:

$$\begin{Bmatrix} -S_{yL} \\ -M_{zL} \\ S_{yR} \\ M_{zR} \end{Bmatrix} = E(1+j\alpha)I \begin{bmatrix} k_{a1}^3 & k_{a2}^3 & k_{a3}^3 & k_{a4}^3 \\ -k_{a1}^2 & -k_{a2}^2 & -k_{a3}^2 & -k_{a4}^2 \\ -k_{a1}^3 e^{k_{a1}L} & -k_{a2}^3 e^{k_{a2}L} & -k_{a3}^3 e^{k_{a3}L} & -k_{a4}^3 e^{k_{a4}L} \\ k_{a1}^2 e^{k_{a1}L} & k_{a2}^2 e^{k_{a2}L} & k_{a3}^2 e^{k_{a3}L} & k_{a4}^2 e^{k_{a4}L} \end{bmatrix} \begin{Bmatrix} A_{11} \\ A_{12} \\ A_{13} \\ A_{14} \end{Bmatrix}, \tag{16a}$$

flexural vibration in (x, z)-plane:

$$\begin{Bmatrix} -S_{zL} \\ -M_{yL} \\ S_{zR} \\ M_{yR} \end{Bmatrix} = E(1+j\alpha)I \begin{bmatrix} k_{a1}^3 & k_{a2}^3 & k_{a3}^3 & k_{a4}^3 \\ k_{a1}^2 & k_{a2}^2 & k_{a3}^2 & k_{a4}^2 \\ -k_{a1}^3 e^{k_{a1}L} & -k_{a2}^3 e^{k_{a2}L} & -k_{a3}^3 e^{k_{a3}L} & -k_{a4}^3 e^{k_{a4}L} \\ -k_{a1}^2 e^{k_{a1}L} & -k_{a2}^2 e^{k_{a2}L} & -k_{a3}^2 e^{k_{a3}L} & -k_{a4}^2 e^{k_{a4}L} \end{bmatrix} \begin{Bmatrix} A_{21} \\ A_{22} \\ A_{23} \\ A_{24} \end{Bmatrix}, \tag{16b}$$

torsional vibration:

$$\begin{Bmatrix} -M_{tL} \\ M_{tR} \end{Bmatrix} = G(1+j\beta)I_p \begin{bmatrix} -k_{b1} & -k_{b2} \\ k_{b1}e^{k_{b1}L} & k_{b2}e^{k_{b2}L} \end{bmatrix} \begin{Bmatrix} B_1 \\ B_2 \end{Bmatrix}, \tag{16c}$$

axial vibration:

$$\begin{Bmatrix} -P_L \\ P_R \end{Bmatrix} = E(1+j\alpha)A_p \begin{bmatrix} -k_{c1} & -k_{c2} \\ k_{c1}e^{k_{c1}L} & k_{c2}e^{k_{c2}L} \end{bmatrix} \begin{Bmatrix} C_1 \\ C_2 \end{Bmatrix}. \tag{16d}$$

Equation (16) can be expressed compactly as flexural vibration in (x, y)-plane:

$$[\mathbf{F}_e]_a = [\mathbf{D}_2]_a \mathbf{A}_a, \tag{17a}$$

flexural vibration in (x, z)-plane:

$$[\mathbf{F}_e]_b = [\mathbf{D}_2]_b \mathbf{A}_b, \tag{17b}$$

torsional vibration:

$$[\mathbf{F}_e]_c = [\mathbf{D}_2]_c \mathbf{A}_c, \tag{17c}$$

axial vibration:

$$[\mathbf{F}_e]_d = [\mathbf{D}_2]_d \mathbf{A}_d, \tag{17d}$$

where $\mathbf{F}_e$ represents the force vector of straight pipe element ends. $[\mathbf{D}_2]_a$, $[\mathbf{D}_2]_b$, $[\mathbf{D}_2]_c$ and $[\mathbf{D}_2]_d$ are the matrices in Equations (16â(16d), respectively.

Substituting Equations (14a), (14b) and (14c), 14d) into Equations (17a), (17b) and (17c), 17d), we can obtain the following equation as

$$[\mathbf{F}_e]_i = [\mathbf{D}_2]_i [\mathbf{D}_1]_i^{-1} [\mathbf{W}_e]_i = [\mathbf{D}_e]_i [\mathbf{W}_e]_i, (i = a, b, c, d). \tag{18}$$

where $[\mathbf{F}_e]_i$ and $[\mathbf{W}_e]_i$ represent the force vector and displacement vector corresponding to 4 vibration motions. In the local coordinate system, $[\mathbf{D}_e]_i$ can be assembled as shown in appendix A, then we can obtain the following relation

$$\mathbf{F}_e = \mathbf{D}_e \mathbf{W}_e, \tag{19}$$

where $\mathbf{D}_e$ is the 12 × 12 non-symmetric dynamic stiffness matrix as a function with frequency in local coordinate system. In a global coordinate system, the dynamic stiffness matrix of a straight pipe element can be expressed as

$$\mathbf{D}_{sg} = \boldsymbol{\lambda}^T \mathbf{D}_e \boldsymbol{\lambda}, \tag{20}$$

where $\boldsymbol{\lambda}$ is the coordinate transformation matrix.

A curved pipe element can be divided into many straight pipe segments, so its dynamic stiffness matrix can be assembled from the straight ones in Equation (20), which is explained in Appendix B. With help of this method, usually referred as transfer matrix method (TMM), we can obtain the global dynamic stiffness matrix $\mathbf{D}_{cg}$ of the entire curved pipe.

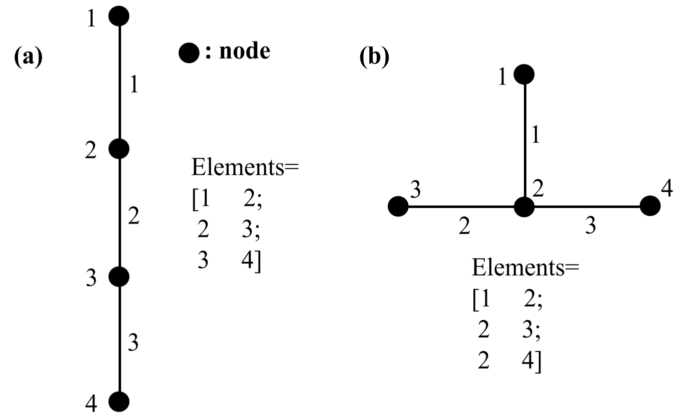

Fig. 2. The relation between elements and nodes in a 3D piping system. (a) Without branch pipe. (b) With branch pipe.

2.1.3. Assembly dynamic stiffness matrix for a 3D piping system

Following the assembly rule as in finite-element method, a global dynamic stiffness matrix $\mathbf{D}_g$ can be obtained by assembling the element dynamic stiffness matrices.

$$\mathbf{D}_g = \sum_{i=1}^{N_{ele}} [\mathbf{D}_{sg}]_i + \sum_{j=1}^{M_{ele}} [\mathbf{D}_{cg}]_j, \tag{21}$$

where N_{ele} and M_{ele} are the number of straight and curved pipe elements, respectively.

The dynamic stiffness assembling process of 3D piping systems with/without branch pipe is illustrated in Fig. 2, and it can be expressed as

$$\mathbf{D}_g = \begin{bmatrix} \mathbf{D}_{11}^1 & \mathbf{D}_{12}^1 & & \\ \mathbf{D}_{21}^1 & \mathbf{D}_{22}^1 + \mathbf{D}_{22}^2 & \mathbf{D}_{23}^2 & \\ & \mathbf{D}_{32}^2 & \mathbf{D}_{33}^2 + \mathbf{D}_{33}^3 & \mathbf{D}_{34}^3 \\ & & \mathbf{D}_{43}^3 & \mathbf{D}_{44}^3 \end{bmatrix}, \tag{22a}$$

$$\mathbf{D}_g = \begin{bmatrix} \mathbf{D}_{11}^1 & \mathbf{D}_{12}^1 & & \\ \mathbf{D}_{21}^1 & \mathbf{D}_{22}^1 + \mathbf{D}_{22}^2 + \mathbf{D}_{22}^3 & \mathbf{D}_{23}^2 & \mathbf{D}_{24}^3 \\ & \mathbf{D}_{32}^2 & \mathbf{D}_{33}^2 & \\ & \mathbf{D}_{42}^3 & & \mathbf{D}_{44}^3 \end{bmatrix}, \tag{22b}$$

where $\mathbf{D}$ represents the dynamic stiffness matrix, the superscript of $\mathbf{D}$ represents the numbering of pipe element, and the two subscripts of $\mathbf{D}$ represents the nodal numberings at both ends of the pipe element.

2.1.4. Boundary conditions for dynamic stiffness matrix of a 3D piping system

Boundary conditions are very important for resonance avoidance. Here, we will demonstrate the influence of some types of supports including elastic hangers, rigid hangers, and locally resonant (LR) structures, on the dynamic stiffness matrix $\mathbf{D}_g$. The constrained dynamic stiffness matrix is represented by $\mathbf{D}_{bc}$. According to different constraint types, $\mathbf{D}_{bc}$ can be obtained by the following procedure described in (1)-

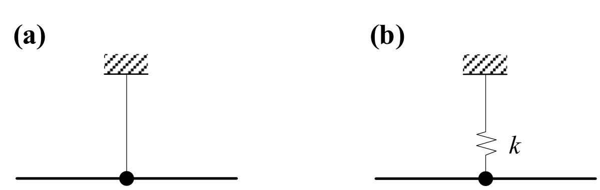

Fig. 3. Typical constraints in a 3D piping system. (a) Rigid hanger. (b) Elastic hanger.

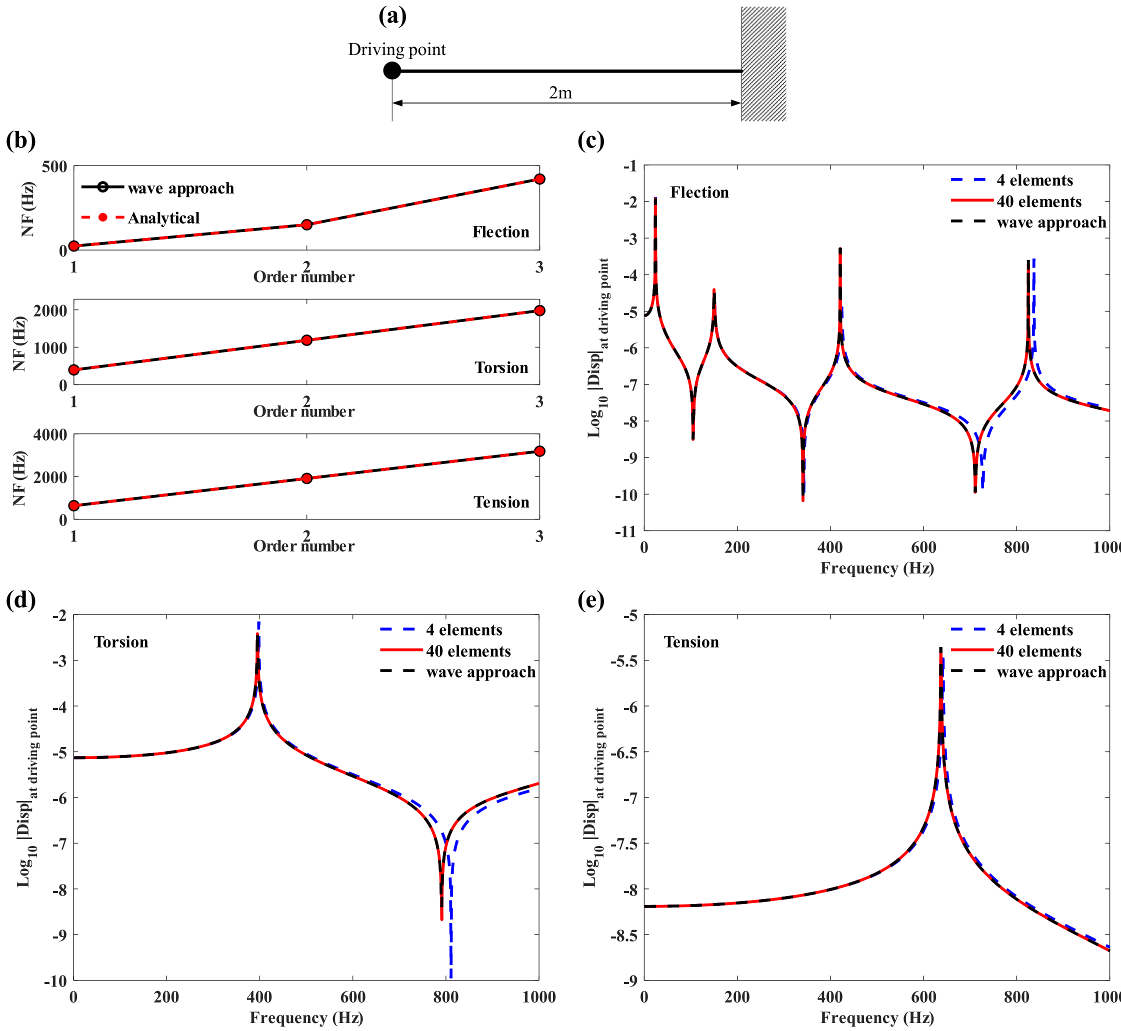

Fig. 4. (a) A cantilevered straight pipe. (b) Comparison of calculated natural frequency (NF). (c) Comparison of flexural vibration frequency response. (d) Comparison of torsional vibration frequency response. (e) Comparison of tensile vibration frequency response. Frequency response calculated by the wave approach and FEM (COMSOL with 4 and 40 elements, respectively).

(3).

(1) When applying a rigid hanger in a 3D piping system, as shown in Fig. 3(a), the rows and columns in the dynamic stiffness matrix $\mathbf{D}_g$ can be eliminated at the location where the displacements are constrained.
(2) The influence of a spring constraint can be considered by adding spring coefficient k to the corresponding degrees of freedom in $\mathbf{D}_g$, as illustrated in Fig. 3(b).

Based on the above explained model, we developed a computational program for vibration analysis of any 3D piping system using MATLAB.

Table 1
Comparison of computing times calculated by wave approach and FEM (COMSOL with 4 and 40 elements, respectively).

	Wave approach	FEM (COMSOL) (4 elements)	FEM (COMSOL) (40 elements)
Computing time (flection)	0.18s	13s	18s
Computing time (torsion)	0.18s	13s	18s
Computing time (tension)	0.18s	13s	18s

This developed framework will be named as modal analysis for short in the following sections.

2.2. Model validation

A cantilevered straight pipe without fluid as shown in Fig. 4(a) is adopted for validating the above model, since it has analytical solutions (flection vibration: $f_r = \beta_r^2\sqrt{\frac{EI}{\rho A}}/2\pi$, $\beta_1 = 1.875/L$, $\beta_2 = 4.694/L$, $\beta_3 = 7.855/L$; torsion vibration: $f_r = \frac{(2r-1)\pi}{2L}\sqrt{G/\rho}/2\pi$; tension vibration: $f_r = \frac{(2r-1)\pi}{2L}\sqrt{E/\rho}/2\pi$; where r is the order number.) for its natural frequencies. The first three natural frequencies (under flection, torsion, and tension, respectively) of the straight pipe calculated via wave approach, and analytical solutions are shown in Fig. 4(b). There is good agreement between the results.

To illustrate the computational efficiency of wave approach, the frequency responses (frequencies from 1 Hz to 1000 Hz with 1 Hz intervals) were calculated using wave approach and FEM (COMSOL with 4 and 40 elements, respectively), as shown in Fig. 4(c–e). In COMSOL, using Beam Interface (Euler-Bernoulli formulation being adopted), frequency domain solver is used to plot the frequency response curve excited by the driving point as shown in Fig. 4(a), and the comparison of computing time is shown in Table 1. In detail, our model has following parameters: the outer diameter D_o is 0.1 m, inter diameter D_i is 0.09 m,

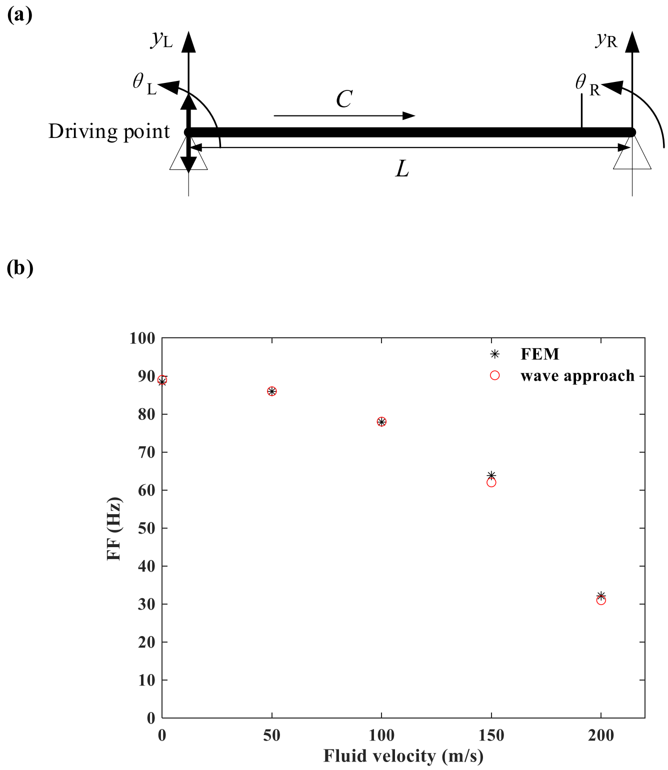

Fig. 5. (a) Nodal displacements in flection vibrations of a straight hinged-hinged pipe conveying fluid. (b) FF of vibrations of a straight hinged-hinged pipe conveying fluid. *: FEM [49]; O: wave approach. In Ref. [49]: D_o = 9.54 mm, D_i = 7.54 mm, E = 208 GPa, ρ_p = 8000 kg/m^3, ρ_f = 1000 kg/m^3, L = 0.5 m, α = 0, β = 0, ν = 0.3 and fluid pressure p = 0 MPa.

Young's modulus E is 208 GPa, pipe mass density ρ_p is 8000 kg/m^3, length L is 2 m, α is 0, β is 0, and the Poisson's ratio ν is 0.3.

From the frequency response curves shown in Fig. 4(c–e), FEM can achieve the accuracy of the wave approach only if enough elements are meshed. As shown in Table 1, the wave approach uses far less computing time than FEM. From the analysis, it is also found that the fundamental frequency (FF) for flexural mode is much smaller than other modes.

In order to validate the accuracy of constant fluid velocity effect based on wave approach, a hinged-hinged straight pipe conveying fluid as shown in Fig. 5(a) is employed. Comparison is shown in Fig. 5(b) with the results obtained by Ref. [49]. There is good agreement between the results.

It should be noted that wave approach is convenient to calculate the displacement response of the node, but wave approach used to solve the vibration mode and stress response of the 3D piping system still remains to be studied. In addition, all vibration governing equations are based on linear theories, which are not applicable to large amplitude vibration.

3. Dynamic characteristics of a 3D piping system

To illustrate the proposed method, we select a general 3D piping system shown in Fig. 6(a) as a basic optimization structure for increasing its FF. The structural parameters of this model include: outer diameter D_o = 0.1 m, inter diameter D_i = 0.09 m, Young's modulus E = 208 GPa, pipe density ρ_p = 8000 kg/m^3, and Poisson's ratio ν = 0.3. To verify the accuracy of 3D piping system without fluid based on wave approach, the frequency responses (frequencies from 0.1 Hz to 10 Hz with 0.001 Hz intervals) were calculated using wave approach and FEM (COMSOL with 25 and 479 elements, respectively), as shown in Fig. 6(b). The accuracy

Table 2
Calculated natural frequencies (Hz) without fluid for different orders and modes.

Force (F) on 6 freedom degrees of node 1						
Order	Flection (xoy-plane)		Flection (xoz-plane)		Tension	Torsion
	Y	θ_z	z	θ_y	u	φ
1	0.468	0.468	0.468	0.468	0.468	0.468
2	0.523	0.523	0.523	0.523	0.523	0.523
3	1.331	1.331	1.331	1.331	1.331	1.331

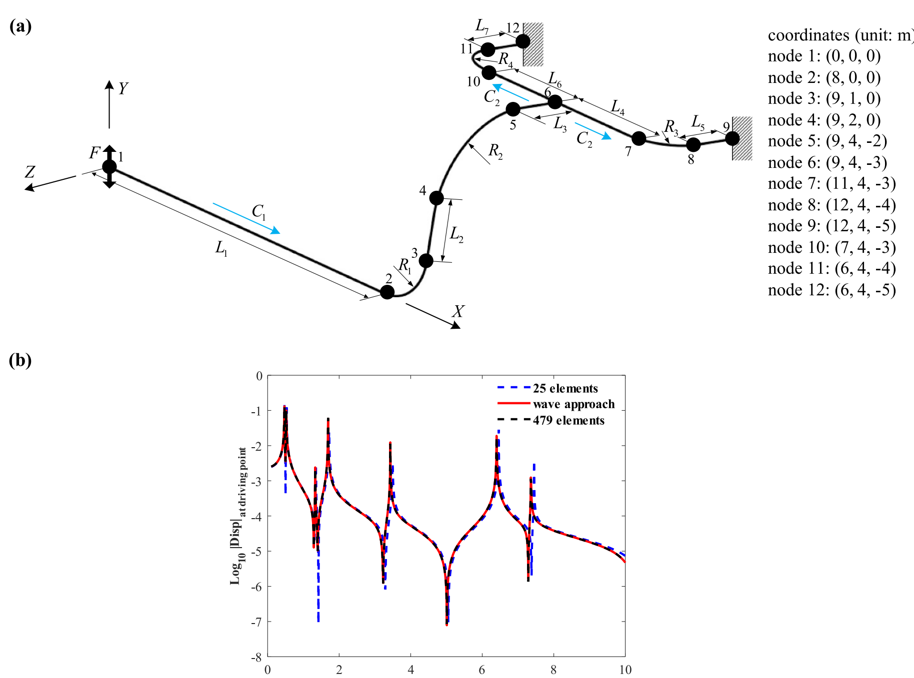

Fig. 6. (a) The analytical model of a 3D piping system with/without fluid. (b) Vibration analysis and verification of 3D piping system without fluid based on wave approach and FEM (COMSOL).

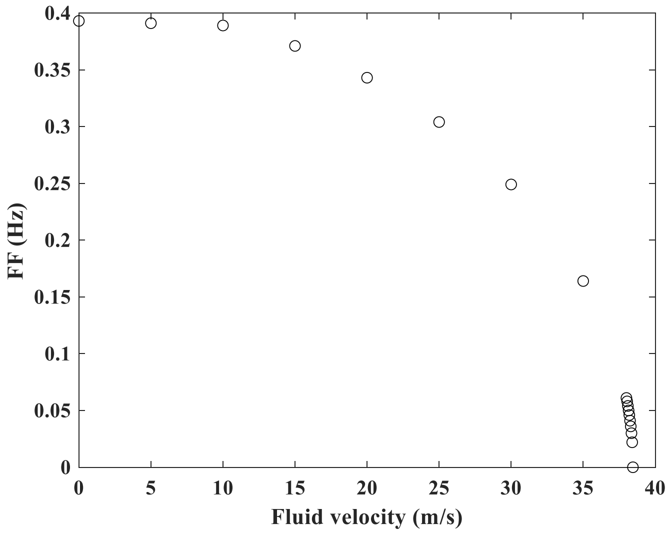

Fig. 7. Dynamic instability of the 3D piping system.

of this calculation program based on wave approach is consistent with the FEM with sufficient number of elements. But, when there is fluid, so far, there is no software can study the frequency response characteristics, which is an advantage of wave approach.

The first three-order natural frequencies of the 3D piping system without fluid calculated by wave approach are shown in Table 2. Due to the coupling of flection, torsion, and tension in the 3D piping system, the same natural frequency can be excited by a force at any degree of freedom at node 1. In our model, the excitation force F is along the Y-direction.

Since the 3D piping system has two branch pipes, the fluid velocity ratio at the junction of the main pipe and branch pipes must satisfy the continuity condition, namely $C_2 = 2C_1\ (D_1^2/D_2^2)$ where C_1, D_1 are the fluid velocity and inner diameter of the main pipe, and C_2, D_2 are the fluid velocity and inner diameter of the branch pipe. The fluid parameters include internal fluid density $\rho_f = 1000\ \mathrm{kg/m^3}$, and internal fluid pressure $p = 0.35$ MPa. The relation between the fluid velocity and FF calculated by the wave approach is shown in Fig. 7 [12]. We can find that the FF hardly changes when the fluid velocity C_1 is below 10 m/s, while the FF decreases sharply as the fluid velocity C_1 increases from 10 m/s to 40 m/s. Furthermore, the critical fluid velocity is close to 38 m/s. The presence of fluid (even when $C_1 = 0$ m/s) can also reduce the FF due to mass effect when optimizing a 3D piping system, therefore fluid must be considered.

4. Optimization examples of a 3D piping system to avoid resonance

4.1. Shape optimization of a 3D piping system

4.1.1. Example description

The 3D piping system (shown in Fig. 6) contains 4 curved pipes with 90° and 7 straight pipes, and the locations of the start (node 1) and end points (nodes 9 and 12) of the 3D piping system are fixed. The lengths of the 7 straight pipes (L_1, L_2, L_3, L_4, L_5, L_6, L_7) and the radii of the 4 curved pipes (R_1, R_2, R_3, R_4) are chosen as optimization variables. The relation between nodal coordinates and pipe sizes are given in Appendix C.

The original sizes of this 3D piping system are assumed to be (unit: m)

$$(L_1, R_1, L_2, R_2, L_3, L_4, R_3, L_5, L_6, R_4, L_7) = (8, 1, 1, 2, 1, 2, 1, 1, 2, 1, 1). \tag{23}$$

In this optimization example, we expect to optimize the 11 variables (L_1, R_1, L_2, R_2, L_3, L_4, R_3, L_5, L_6, R_4, L_7) of the 3D piping system to improve the FF, which in fact characterize the shape of the 3D piping system. The detail of the dynamic stiffness is given in Appendix B. Briefly, the dynamic stiffness matrices $\mathbf{D}_{sg}$ of the straight pipe elements and $\mathbf{D}_{cg}$ of the curved pipe element are expressed with two end or center coordinates, the global dynamic stiffness matrix $\mathbf{D}_g$ of the whole 3D piping system can then be obtained.

Furthermore, the 11 variables should satisfy some certain constraints in the manufacturing process [47]. For example, the curved pipe is machined by bending instrument, the bending radius R should be 1.5 times large than the diameter, and the length L of the straight pipe must be 2.5 times larger than the diameter. Assuming that the design space for the 3D piping system is [12 m, 4 m, 5 m], the 11 variables ($\mathbf{X}$=(L_1, L_2, L_3, L_4, L_5, L_6, L_7, R_1, R_2, R_3, R_4)) must satisfy the following relations: $L_{min} \le L_1 \le 12$ m, $L_{min} \le L_2 \le 4$ m, $L_{min} \le L_3 \le 5$ m, $L_{min} \le L_4 \le 6$ m, $L_{min} \le L_5 \le 5$ m, $L_{min} \le L_6 \le 6$ m, $L_{min} \le L_7 \le 5$ m, $R_{min} \le R_1 \le 4$ m, $R_{min} \le R_2 \le 4$ m, $R_{min} \le R_3 \le 5$ m and $R_{min} \le R_4 \le 5$ m where L_{min} represents $2.5D_o$, and R_{min} represents $1.5D_o$.

Since the task of a 3D piping system is to deliver fluid from one starting point to both ending points, the both ending points are fixed, which are (unit: m)

$$P_{end}^1 = \text{node } 9 = [12, 4, -5], \tag{24a}$$

$$P_{end}^2 = \text{node } 12 = [6, 4, -5]. \tag{24b}$$

Therefore, the constraint conditions on the 11 variables are expressed as (unit: m)

$$\begin{cases} L_1 + R_1 + L_4 + R_3 = 12 \\ R_1 + L_2 + R_2 = 4 \\ -R_2 - L_3 - R_3 - L_5 = -5 \\ L_1 + R_1 - L_6 - R_4 = 6 \\ -R_2 - L_3 - R_4 - L_7 = -5 \end{cases}. \tag{25}$$

For the vibration of the piping system, resonance must be avoided, particularly, the natural frequency of the engine cannot coincide with that of the pipe. Therefore, we take maximizing the FF of the 3D piping system as the optimization target. The natural frequency of a 3D pipeline system can be obtained from the condition that determinant of $\mathbf{D}_g(\omega)$ should vanish at the natural frequency:

$$|\mathbf{D}_g(\omega)| = 0. \tag{26}$$

To compute the natural frequencies from Equation (26), we can use a proper root-finding algorithm [13–15]. Here, we select to sweep the parameter ω. To avoid resonance, the first natural frequency f_1 of the 3D piping system should be far away from external excitation frequency f_e (e.g. 0.5Hz), Finding the max (f_1−f_e) means to find the min −(f_1−f_e), where f_1 is the FF of the 3D piping system. This shape optimization model for avoiding resonance of a 3D piping system can be expressed as

$$\begin{array}{l} \min : -[f_1(\mathbf{X}) - f_e] \\ s.t. \\ constraints \end{array} \tag{27}$$

The optimization is performed based on the well-known genetic algorithm (GA). During the optimization process, the f_1 (i.e. FF) is calculated by using the program based on wave approach. The general optimization solution flowchart of the 3D piping system based on shape optimization is shown in Figure D1.

4.1.2. Numerical results of shape optimization

Following the above optimization process, in the case of the maximal FF, which is derived from the minimum objective function value, we can obtain a shape shown in Fig. 8(b) with the 11 shape variables (unit: m):

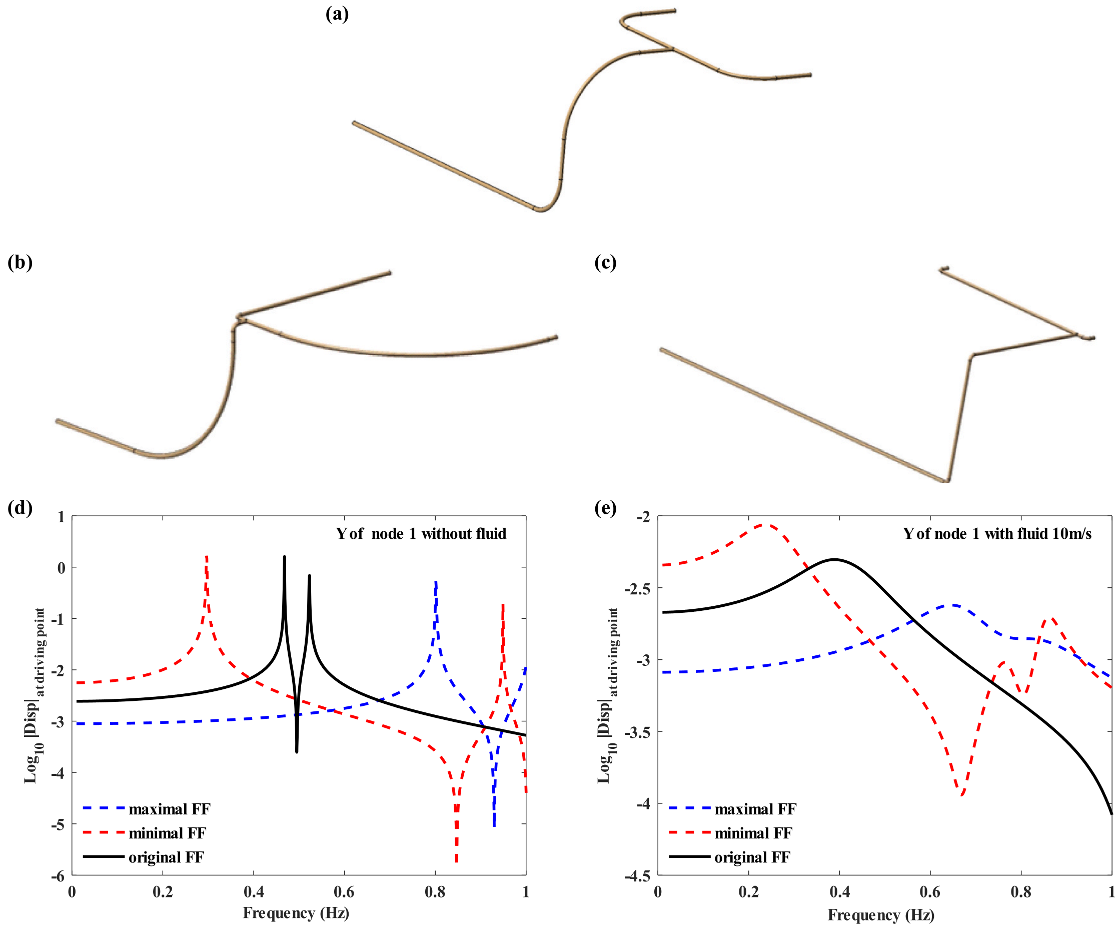

Fig. 8. (a) The model with original FF. (b) The model with maximal FF. (c) The model with minimal FF. (d) Frequency response comparison of models in (a), (b) and (c) without fluid. (e) Frequency response comparison of models in (a), (b) and (c) with flowing fluid (C_1 = 10 m/s).

$$(L_1, R_1, L_2, R_2, L_3, L_4, R_3, L_5, L_6, R_4, L_7) = (2.80, 3.60, 0.25, 0.15, 0.25, 1.25, 4.35, 0.25, 0.25, 0.15, 4.45). \tag{28}$$

In the case of minimal FF, for comparing, we can obtain a shape shown in Fig. 8(c) with the 11 shape variables (unit: m):

$$(L_1, R_1, L_2, R_2, L_3, L_4, R_3, L_5, L_6, R_4, L_7) = (11.45, 0.15, 3.70, 0.15, 4.45, 0.25, 0.15, 0.25, 5.45, 0.15, 0.25). \tag{29}$$

The results show that maximal and minimal FF without fluid are 0.80 Hz and 0.30 Hz, respectively, as illustrated in Fig. 8(d). In order to reveal the effect of fluid velocity on the vibration of the piping system, we set the fluid velocity C_1 as 10 m/s, and the optimized shapes of the piping system with maximal and minimal FF are similar to the shapes without fluid, as shown in Fig. 8(b) and (c). Nevertheless, the maximal and minimal FF with fluid (C_1 = 10 m/s) are 0.65 Hz and 0.22 Hz, respectively, as illustrated in Fig. 8(e). Compared to the case without fluid, it seems that the fluid velocity has less effect on the optimized shape of the piping system, but has significant effect on the FF.

Fig. 8(d) shows the frequency response curves of three models with the maximal, minimal, and original FF, illustrating the effect of shape optimization on the vibration of a 3D piping system. Moreover, the frequency response curves of the piping system with flowing fluid (C_1 = 10 m/s) are illustrated in Fig. 8(e), showing that fluid velocity can reduce the FF as well as the vibration magnitude. In this optimized model, the maximal FF (Fig. 8(b)) is nearly 3 times higher than the minimal FF (Fig. 8(c)).

4.2. *Rigid hanger location optimization of a 3D piping system*

Another method to avoid resonance is to mount hangers on the piping system, such as rigid hangers and elastic hangers. Firstly, we optimize the location of a rigid hanger, and then, for better optimization effect, we optimize the location of four rigid hangers.

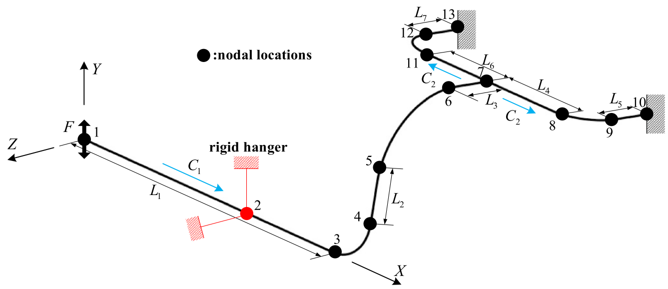

Fig. 9. Analytical model of a 3D piping system with one rigid hanger.

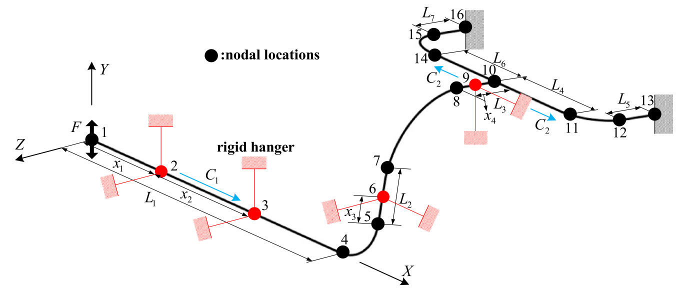

Fig. 11. Analytical model of a 3D piping system with 4 rigid hangers.

Table 3
Comparison of calculated results.

	no fluid		fluid velocity $C_1 = 10$ m/s	
	numbering and location	FF (Hz)	numbering and location	FF (Hz)
maximal FF	No.1, 3.6291 m	1.30	No.1, 3.3238 m	1.03
minimal FF	No.5, 0.6790 m	0.47	No.5, 0.3931 m	0.39

4.2.1. Example of one rigid hanger location optimization

When mounting one rigid hanger on the pipe, it would be beneficial to tell which straight pipe and where this rigid hanger should be mounted. An illustrated scheme of installation is shown in Fig. 9.

When rigid hanger is mounted on a straight pipe, it will restrain the flexural vibration displacement at the mounted location (node 2 in Fig. 9). The direction of the constrained displacement depends on the numbering of the straight pipes. When rigid hangers are mounted on the pipes (L_1, L_4, L_6), the hangers can restrain the displacement in the (Y, Z) direction. When rigid hangers are mounted on the pipes (L_3, L_5, L_7), the hangers can restrain the displacements in (X, Y) directions. When rigid hangers are mounted on the pipe L_2, the hangers can restrain the displacement in the (X, Z) direction. Consequently, the mounted location $\mathbf{W}_{\mathrm{rh}}$ (node 2 in Fig. 9) of the rigid hanger on the straight pipe can be coded as

$$\mathbf{W}_{\mathrm{rh}} = \mathbf{W}_{n1} + \mathbf{e}_n \cdot x_n \ (n = 1,2,3,4,5,6,7), \tag{30}$$

where $\mathbf{W}_{n1}$ and $\mathbf{e}_n$ are the first nodal location and the axial unit vector of the numbering n straight pipe, respectively. This rigid hanger optimization model for avoiding resonance of a 3D piping system can be expressed as

$$\begin{aligned} &\min : -[f_1(n, x_n) - f_e] \\ &\text{s.t. } n \in \{1,2,3,4,5,6,7\}, \\ &L_{\min} \le x_n \le L_n - L_{\min} \end{aligned} \tag{31}$$

The corresponding optimization solution flowchart of a 3D piping system based on one rigid hanger location optimization is shown in Figure D2.

As shown in Table 3, following the above optimization procedure, in the case of the maximal FF (i.e. f_1), which derived from the minimum objective function value, we obtained the straight pipe numbering (n) and the mounted location (x_n) of the piping system. For comparing the optimization effect, we also obtained the result in the case of the minimal FF. When the 3D piping system conveys fluid (C = 10 m/s), the optimization result with the maximal FF is shown in Table 3, and the result with minimal FF is obtained for comparing.

Meanwhile, from Table 3, it can be found that the fluid flow hardly affects the optimization results of numbering (n) and mounted location (x_n), but reduces the FF. The optimization results shows that when the location of rigid hanger is closed to fixed end, it can hardly influence the FF, and the optimized rigid hanger location is near 3.6 m away from the first node of No.1 straight pipe.

In addition, we still investigate the influence of elastic hanger on the fundamental frequency, as shown in Fig. 10. For this 3D piping system, When the stiffness of elastic hanger is greater than 10 ˆ 6 N/m, the fundamental frequency tends to be stable and consistent with that of rigid hanger, thus the elastic hanger can be regarded as a rigid one. As Fig. 10 shows, the rigid hanger changes the fundamental frequency more obviously than the elastic hanger, and the optimization effect is better. Therefore, in order to optimize the target, we choose rigid hangers instead of elastic hangers.

It should be noted that the present study only investigated the role of one rigid hanger on the fundamental frequency of a 3D piping system. In order to further improve the FF, more rigid hangers should be mounted on the piping system. The optimal locations of these rigid hangers can also be found by genetic algorithm.

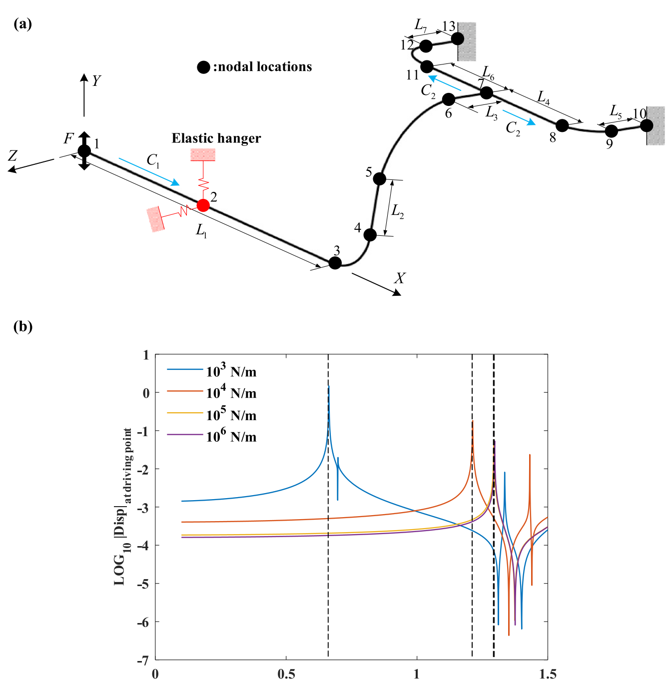

Fig. 10. (a) Analytical model of a 3D piping system with one elastic hanger, the location is 3.6291 m away from node 1. (b) The relationship between FF and four elastic hangers (10ˆ3 N/m, 10ˆ4 N/m, 10ˆ5 N/m, 10ˆ6 N/m, respectively) with the model shown in (a).

4.2.2. Example of more rigid hangers' location optimization

To illustrate the effect of more rigid hangers on increasing the FF of a 3D piping system, four rigid hangers are adopted: two are mounted on the pipe section (L_1), one is mounted on the pipe section (L_2), and one is mounted on the pipe section (L_3), as shown in Fig. 11. The model for location optimization of four rigid hangers can be expressed as

Table 4
Comparison of calculated results.

	no fluid		fluid velocity $C_1 = 10$ m/s	
	Location (m)	FF(Hz)	Location (m)	FF(Hz)
maximal FF	2.0156,2.7295,0.3119,0.2602	8.50	2.1405,3.8607,0.5915,0.2542	7.57
minimal FF	7.3933,0.3566,0.4742,0.5235	1.70	7.1974,0.5526,0.3750,0.7500	1.43

$$\begin{array}{l} \min: -[f_1(x_1,x_2,x_3,x_4) - f_e] \\ s.t. \\ L_{\min} \le x_1 \le L_1 - 2\cdot L_{\min} \\ L_{\min} \le x_2 \le L_1 - 2\cdot L_{\min} \\ L_{\min} \le x_3 \le L_2 - L_{\min} \\ L_{\min} \le x_4 \le L_3 - L_{\min} \end{array} . \tag{32}$$

The corresponding optimization solution flowchart based on four rigid hanger locations optimization is shown in Figure D3.

Results of four rigid hangers' location optimization are shown in Table 4, and we can find that the maximal FF (i.e. f_1) (no fluid, 8.50 Hz; $C_1 = 10$ m/s, 7.57 Hz) with optimized positions is much greater than the minimal, indicating that the FF of 3D piping system can be more far away from excitation frequency. Nevertheless, from an economic perspective, we will focus on the trade-off between the maximal resonance avoidance and minimal hanger number in our future work.

In our work, compared with the shape optimization (0.30 Hz ~ 0.80 Hz), the effect of rigid hanger location optimization (one rigid hanger: 0.47 Hz ~ 1.30 Hz, Table 3; four rigid hangers: 1.70 Hz ~ 8.50 Hz, Table 4) dominates on improving the fundamental frequency of the 3D piping system. The effect of adjusting the fundamental frequency to avoid vibration by shape optimization is relatively low, and the significance of shape optimization is that it can provide a solution when additional hangers cannot be installed in a confined space. By rigid hangers' location optimization, the effect of changing the fundamental frequency is more obvious, and the effect of vibration avoidance is better.

5. Conclusion

In this paper, a systematic method for global optimization design of a 3D piping system is proposed and numerically validated. Based on wave approach initially given by Koo and Park [11], we extended this approach to 3D liquid conveying piping systems to estimate the fundamental frequency in a fast and efficient way. Combining with genetic algorithm, shape optimization can be used to increase fundamental frequency of a piping system if rigid hangers are not available; in contrast, the fundamental frequency can be improved more efficiently with rigid hangers of optimized locations. Our proposed method can provide an efficient and accurate vibration analysis for a general 3D liquid conveying pipe system in its pre-designed stage.

Credit author statement

Xiangliang Wang: Methodology, Investigation, Validation, Software, Writing – original draft. **Pingzhang Zhou**: Methodology, Investigation, Validation, Software, Writing. **Yun Ma**: Supervision, Writing – review & editing. **Gengkai Hu**: Supervision, Conceptualization, Resources, Writing – review & editing.

Declaration of competing interest

The authors declare that they have no known competing financial interests or personal relationships that could have appeared to influence the work reported in this paper.

Data availability

Data will be made available on request.

Acknowledgement

Financial support from the National Natural Science Foundation of China (Grants No. 11632003, No. 11972083, No. 11991030, No. 12002042) is acknowledged.

Appendix A

These 4 vibration motions can be assembled into the 12×12 dynamic stiffness matrix $\mathbf{D}_{sg}$ of straight pipe element as shown in Figure A1, and the corresponding relation between the numberings and 12 nodal degrees of freedom of straight pipe element ends is shown in table A1.

Table A1
Corresponding relation between the numberings and 12 nodal degrees of freedom.

1	2	3	4	5	6	7	8	9	10	11	12
u_L	y_L	z_L	φ_L	θ_{yL}	θ_{zL}	u_R	y_R	z_R	φ_R	θ_{yR}	θ_{zR}

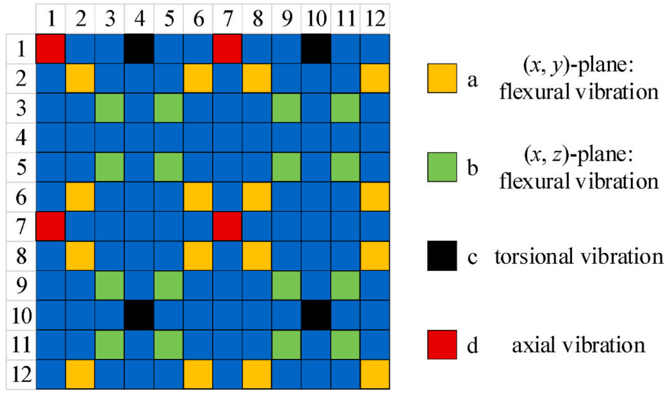

Fig. A1. Assembled dynamic stiffness matrix of straight pipe element

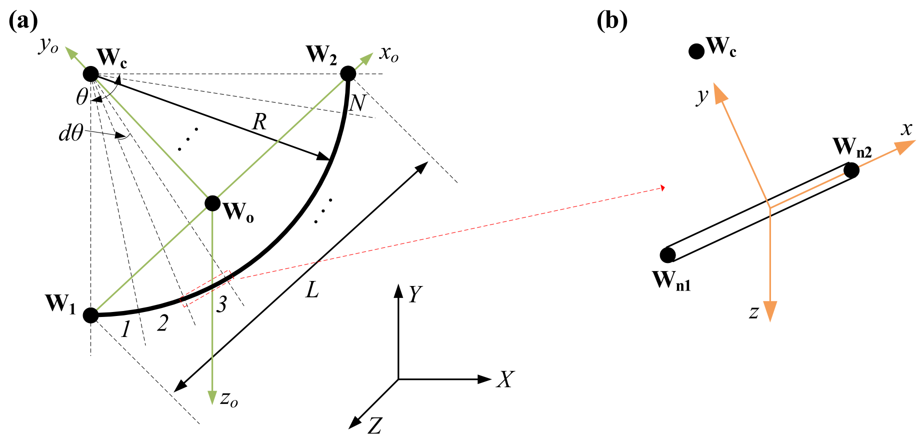

Fig. B1. (a) Segments of a curved pipe. (b). Single segment.

Appendix B

When calculating the dynamic stiffness of the curved pipe, it is necessary to find the coordinates of the both ends ($\mathbf{W}_1$, $\mathbf{W}_2$) and the center-point ($\mathbf{W}_c$) of the curved pipe in the global coordinate system (X, Y, Z). As shown in Figure B1(a), we divide the curved pipe into N equal segments, and each segment is considered as a straight pipe. The parameters of the curved pipe can be expressed as

$$\begin{aligned} &R=|\mathbf{W}_c-\mathbf{W}_1|,\\ &L=|\mathbf{W}_2-\mathbf{W}_1|,\\ &\mathbf{W}_o=(\mathbf{W}_2+\mathbf{W}_1)/2,\\ &\theta=2\times\sin^{-1}(L/(2R)),\\ &d\theta=\theta/N, \end{aligned} \tag{B1}$$

where R and θ are the radius and radian of the curved pipe, respectively, L and $\mathbf{W}_o$ are the Length and midpoint of the line connecting the both ends ($\mathbf{W}_1$, $\mathbf{W}_2$), respectively, and $d\theta$ is the radian of one part of the curved pipe.

In the local coordinate system (x_o, y_o, z_o), the center-point location of the curved pipe can be expressed as

$$\begin{aligned} &x_c=0,\\ &y_c=\left[R^2-(L/2)^2\right]^{1/2},\\ &z_c=0. \end{aligned} \tag{B2}$$

and the locations of each segment end can be expressed as

$$\left.\begin{aligned} x_n&=x_c-R\sin(\theta/2-nd\theta)\\ y_n&=y_c-R\cos(\theta/2-nd\theta)\\ z_n&=z_c \end{aligned}\right\}(n=0,1,2\cdots N). \tag{B3}$$

The locations of each segment end in the local coordinate system (x_o, y_o, z_o) can be transformed into the global coordinate system (X, Y, Z) as

$$\mathbf{W}_n=\mathbf{T}_3{}^{\mathrm{T}}\bullet\mathbf{w}_n+\mathbf{W}_o \tag{B4}$$

where $\mathbf{w}_n$ is the locations of each segment end in the local coordinate system (x_o, y_o, z_o), and $\mathbf{T}_3$ is the coordinate transformation matrix from the global coordinate system (X, Y, Z) into the local coordinate system (x_o, y_o, z_o).

As shown in Figure B1(b), according to the coordinates of the both ends ($\mathbf{W}_{n1}$, $\mathbf{W}_{n2}$) of the segment and the center-point ($\mathbf{W}_c$) of the curved pipe, the dynamic stiffness transformation matrix $\boldsymbol{\lambda}$ from the global coordinate system (X, Y, Z) into the local coordinate system (x, y, z) can be confirmed. The dynamic stiffness matrix of a segment in the global coordinate system (X, Y, Z) can be expressed as

$$\mathbf{D}_{cn}=\boldsymbol{\lambda}^{T}\mathbf{D}_{e}\boldsymbol{\lambda}=\begin{bmatrix}\mathbf{K}_1 & \mathbf{K}_2\\ \mathbf{K}_3 & \mathbf{K}_4\end{bmatrix} \tag{B5}$$

where $\mathbf{K}_i$ (i = 1,2,3,4) is the partitioned dynamic stiffness matrix from $\mathbf{D}_e$. Using the TMM theory,

$$\begin{bmatrix}-\mathbf{F}_L\\ \mathbf{F}_R\end{bmatrix}_n=\begin{bmatrix}\mathbf{K}_1 & \mathbf{K}_2\\ \mathbf{K}_3 & \mathbf{K}_4\end{bmatrix}\begin{bmatrix}\mathbf{W}_L\\ \mathbf{W}_R\end{bmatrix}_n \tag{B6}$$

can be expressed as

$$\begin{bmatrix}\mathbf{W}_R\\ \mathbf{F}_R\end{bmatrix}_n=\begin{bmatrix}-\mathbf{K}_2^{-1}\mathbf{K}_1 & -\mathbf{K}_2^{-1}\\ \mathbf{K}_3-\mathbf{K}_4\mathbf{K}_2^{-1}\mathbf{K}_1 & -\mathbf{K}_4\mathbf{K}_2^{-1}\end{bmatrix}\begin{bmatrix}\mathbf{W}_L\\ \mathbf{F}_L\end{bmatrix}_n (n=1,2,\cdots N), \tag{B7}$$

where $\mathbf{W}_R$ and $\mathbf{W}_L$ are displacements of both ends of the segment, and $\mathbf{F}_R$ and $\mathbf{F}_L$ are forces of both ends of the segment. Transfer matrix $\mathbf{T}_n$ of the segment can be expressed as

$$\mathbf{T}_n=\begin{bmatrix}-\mathbf{K}_2^{-1}\mathbf{K}_1 & -\mathbf{K}_2^{-1}\\ \left(\mathbf{K}_3-\mathbf{K}_4\mathbf{K}_2^{-1}\mathbf{K}_1\right) & -\mathbf{K}_4\mathbf{K}_2^{-1}\end{bmatrix}_n. \tag{B8}$$

Using the chain rule, transfer matrix $\mathbf{T}_c$ for both ends of the curved pipe is expressed as

$$\begin{bmatrix}\mathbf{W}_R\\ \mathbf{F}_R\end{bmatrix}_N=[\mathbf{T}]_N[\mathbf{T}]_{N-1}\cdots[\mathbf{T}]_1\begin{bmatrix}\mathbf{W}_L\\ \mathbf{F}_L\end{bmatrix}_1=\mathbf{T}_c\begin{bmatrix}\mathbf{W}_L\\ \mathbf{F}_L\end{bmatrix}_1=\begin{bmatrix}\mathbf{T}_1 & \mathbf{T}_2\\ \mathbf{T}_3 & \mathbf{T}_4\end{bmatrix}\begin{bmatrix}\mathbf{W}_L\\ \mathbf{F}_L\end{bmatrix}_1. \tag{B9}$$

From Equation (B9), the dynamic stiffness matrix $\mathbf{D}_{cg}$ for the curved pipe can be expressed as

$$\begin{bmatrix}-\mathbf{F}_L\\ \mathbf{F}_R\end{bmatrix}=\begin{bmatrix}\mathbf{T}_2^{-1}\mathbf{T}_1 & -\mathbf{T}_2^{-1}\\ \left(\mathbf{T}_3-\mathbf{T}_4\mathbf{T}_2^{-1}\mathbf{T}_1\right) & \mathbf{T}_4\mathbf{T}_2^{-1}\end{bmatrix}\begin{bmatrix}\mathbf{W}_L\\ \mathbf{W}_R\end{bmatrix}=\mathbf{D}_{cg}\begin{bmatrix}\mathbf{W}_L\\ \mathbf{W}_R\end{bmatrix}. \tag{B10}$$

Appendix C

Table C1
Coordinates of nodes.

Nodes	Coordinates (unit: m)
node1	[0, 0, 0]
node2	[L_1, 0, 0]
node3	[L_1+R_1, R_1, 0]
node4	[L_1+R_1, R_1+L_2, 0]
node5	[L_1+R_1, $R_1+L_2+R_2$, $-R_2$]
node6	[L_1+R_1, $R_1+L_2+R_2$, $-R_2-L_3$]
node7	[$L_1+R_1+L_4$, $R_1+L_2+R_2$, $-R_2-L_3$]
node8	[$L_1+R_1+L_4+R_3$, $R_1+L_2+R_2$, $-R_2-L_3-R_3$]
node9	[$L_1+R_1+L_4+R_3$, $R_1+L_2+R_2$, $-R_2-L_3-R_3-L_5$]
node10	[$L_1+R_1-L_6$, $R_1+L_2+R_2$, $-R_2-L_3$]
node11	[$L_1+R_1-L_6-R_4$, $R_1+L_2+R_2$, $-R_2-L_3-R_4$]
node12	[$L_1+R_1-L_6-R_4$, $R_1+L_2+R_2$, $-R_2-L_3-R_4-L_7$]

Appendix D

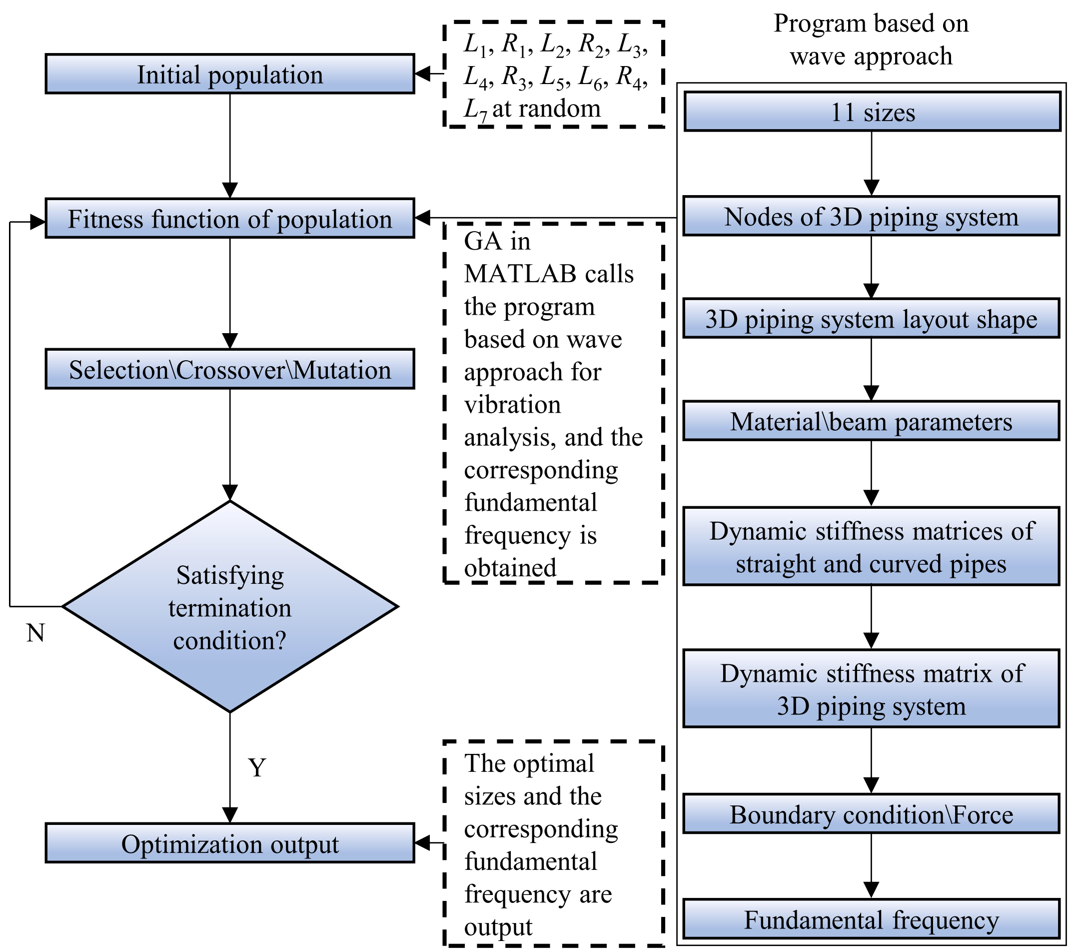

Fig. D1. Shape optimization flowchart of a 3D piping system.

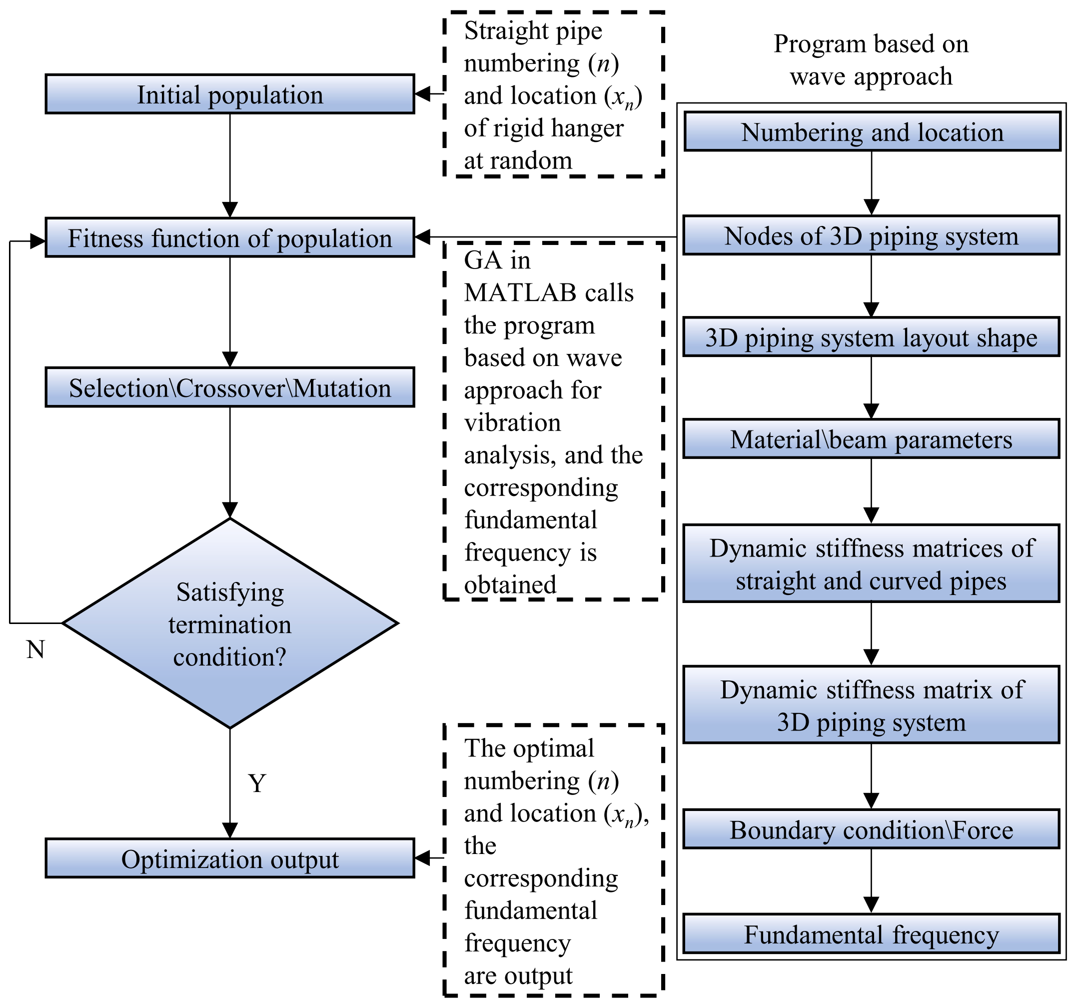

Fig. D2. One rigid hanger location optimization flowchart of a 3D piping system.

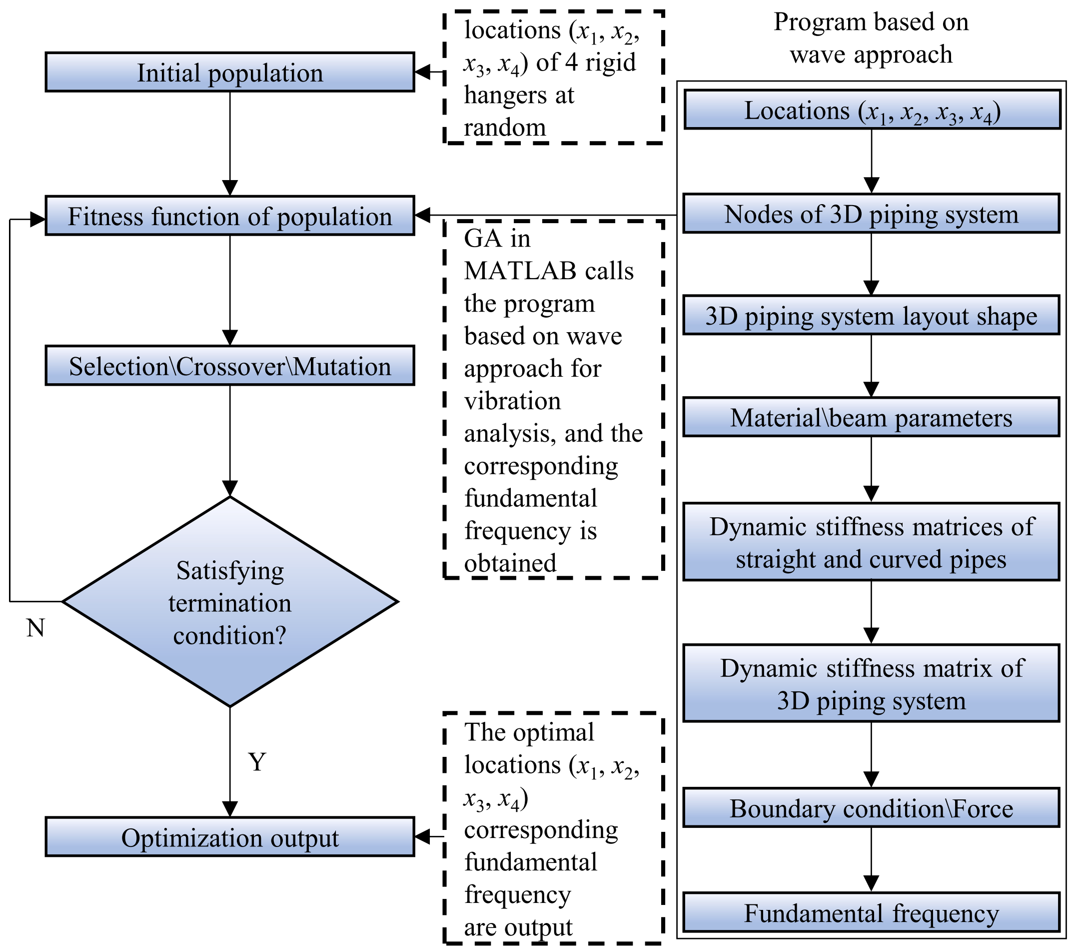

Fig. D3. 4 rigid hanger locations optimization flowchart of a 3D piping system.

References

[1] H. Shen, J. Wen, D. Yu, X. Wen, The vibrational properties of a periodic composite pipe in 3D space, J. Sound Vib. 328 (1–2) (2009) 57–70.

[2] Y. Li, H. Shen, L. Zhang, Y. Su, D. Yu, Control of low-frequency noise for piping systems via the design of coupled band gap of acoustic metamaterials, Phys. Lett. 380 (29–30) (2016) 2322–2328.

[3] M.P. Païdoussis, Fluid-Structure Interactions Slender Structures and Axial Flow, second ed., Academic Press, 2014.

[4] H. Shen, J. Wen, D. Yu, B. Yuan, X. Wen, Stability of fluid-conveying periodic shells on an elastic foundation with external loads, J. Fluid Struct. 46 (2014) 134–148.

[5] H. Shen, J. Wen, M.P. Païdoussis, D. Yu, M. Asgari, X. Wen, Control of sound and vibration for cylindrical shells by utilizing a periodic structure of functionally graded material, Phys. Lett. 376 (45) (2012) 3351–3358.

[6] B. Hu, Z. Zhang, D. Yu, J. Liu, F. Zhu, Broadband bandgap and shock vibration properties of acoustic metamaterial fluid-filled pipes, J. Appl. Phys. 128 (20) (2020), 205103.

[7] T. Ren, Z. Zhu, G.M. Dimirovski, Z. Gao, X. Sun, H. Yu, A new pipe routing method for aero-engines based on genetic algorithm, Proc. Inst. Mech. Eng., Part G 228 (3) (2013) 424–434.

[8] A.K. Misra, M.P. Païdoussis, K.S. Van, On the dynamics of curved pipes transporting fluid. Part I: Inextensible theory, J. Fluid Struct. 2 (3) (1988) 221–244.

[9] A.K. Misra, M.P. Païdoussis, K.S. Van, On the dynamics of curved pipes transporting fluid Part II: Extensible theory, J. Fluid Struct. 2 (3) (1988) 245–261.

[10] H.L. Dai, L. Wang, Q. Qian, J. Gan, Vibration analysis of three-dimensional pipes conveying fluid with consideration of steady combined force by transfer matrix method, Appl. Math. Comput. 219 (5) (2012) 2453–2464.

[11] G.H. Koo, Y.S. Park, Vibration analysis of a 3-dimensional piping system conveying fluid by wave approach, Int. J. Pres. Ves. Pip. 67 (3) (1996) 249–256.

[12] G.H. Koo, B. Yoo, Dynamic characteristics of KALIMER IHTS hot leg piping system conveying hot liquid sodium, Int. J. Pres. Ves. Pip. 77 (11) (2000) 679–689.

[13] U. Lee, H. Oh, The spectral element model for pipelines conveying internal steady flow, Eng. Struct. 25 (8) (2003) 1045–1055.

[14] U. Lee, J. Park, Spectral element modelling and analysis of a pipeline conveying internal unsteady fluid, J. Fluid Struct. 22 (2) (2006) 273–292.

[15] U. Lee, I. Jang, H. Go, Stability and dynamic analysis of oil pipelines by using spectral element method, J. Loss Prev. Process. Ind. 22 (6) (2009) 873–878.

[16] W. Chen, K. Zhou, L. Wang, Z. Yin, Geometrically exact model and dynamics of cantilevered curved pipe conveying fluid, J. Sound Vib. (2022) 534.

[17] W. Chen, H. Dai, Q. Jia, L. Wang, Geometrically exact equation of motion for large-amplitude oscillation of cantilevered pipe conveying fluid, Nonlinear Dynam. 98 (3) (2019) 2097–2114.

[18] D. Hong, J. Tang, G. Ren, Dynamic modeling of mass-flowing linear medium with large amplitude displacement and rotation, J. Fluid Struct. 27 (8) (2011) 1137–1148.

[19] K. Zhou, Q. Ni, W. Chen, H.L. Dai, P. Hagedorn, L. Wang, Static equilibrium configuration and nonlinear dynamics of slightly curved cantilevered pipe conveying fluid, J. Sound Vib. (2021) 490.

[20] K. Zhou, H.R. Yi, H.L. Dai, H. Yan, Z.L. Guo, F.R. Xiong, Q. Ni, P. Hagedorn, L. Wang, Nonlinear analysis of L-shaped pipe conveying fluid with the aid of absolute nodal coordinate formulation, Nonlinear Dynam. 107 (1) (2021) 391–412.

[21] H. Dai, Y. He, K. Zhou, Z. Peng, L. Wang, P. Hagedorn, Utilization of nonlinear vibrations of soft pipe conveying fluid for driving underwater bio-inspired robot, Appl. Math. Mech. 43 (7) (2022) 1109–1124.

[22] J.-R. Yuan, H. Ding, Dynamic model of curved pipe conveying fluid based on the absolute nodal coordinate formulation, Int. J. Mech. Sci. (2022) 232.

[23] H. Sui, W. Niu, Branch-pipe-routing approach for ships using improved genetic algorithm, Front Mech Eng Prc 11 (3) (2016) 316–323.

[24] Z. Dong, Y. Lin, Ship pipe routing method based on genetic algorithm and cooperative coevolution, J Ship Prod Des 33 (2) (2017) 122–134.

[25] Y. Qu, D. Jiang, Q. Yang, Branch pipe routing based on 3D connection graph and concurrent ant colony optimization algorithm, J. Intell. Manuf. 29 (7) (2016) 1647–1657.

[26] K. Chen, Y. Zhao, Y. Liu, H. Yu, S. Huang, Optimization method for spatial route adjustment of multi-bends pipes considering assembly demands, Assemb. Autom. 42 (3) (2022) 319–332.

[27] Q. Liu, C. Wang, Pipe-assembly approach for aero-engines by modified particle swarm optimization, Assemb. Autom. 30 (4) (2010) 365–377.
[28] P. Gao, T. Yu, Y. Zhang, J. Wang, J. Zhai, Vibration analysis and control technologies of hydraulic pipeline system in aircraft: a review, Chin. J. Aeronaut. 34 (4) (2021) 83–114.
[29] Z. Tang, Z. Lu, D. Li, F. Zhang, Optimal design of the positions of the hoops for a hydraulic pipelines system, Nucl. Eng. Des. 241 (12) (2011) 4840–4855.
[30] W. Wang, C. Zhou, H. Gao, Z. Zhang, Application of non-probabilistic sensitivity analysis in the optimization of aeronautical hydraulic pipelines, Struct Multidiscip O 57 (6) (2017) 2177–2191.
[31] Z. Zhang, C. Zhou, W. Wang, Z. Yue, Optimization design of aeronautical hydraulic pipeline system based on non-probabilistic sensitivity analysis, Proc. Inst. Mech. Eng., Part O 233 (5) (2019) 815–825.
[32] A.H.M. Kwong, K.A. Edge, A method to reduce noise in hydraulic systems by optimizing pipe clamp locations, Proc. Inst. Mech. Eng., Part I 212 (14) (1998) 267–280.
[33] X. Liu, W. Sun, Y. Gao, H. Ma, Optimization of pipeline system with multi-hoop supports for avoiding vibration, based on particle swarm algorithm, Proc. Inst. Mech. Eng., Part C 235 (9) (2021) 1524–1538.
[34] D. Wang, W. Sun, Z. Gao, H. Ma, Optimization of spatial pipeline with multi-hoop supports for avoiding resonance problem based on genetic algorithm, Sci. Prog. 105 (1) (2022) 1–23.
[35] Z. Liu, X. Zhang, Y. Mao, Y.Y. Zhu, Z. Yang, C.T. Chan, P. Sheng, Locally resonant sonic materials, Science 289 (5485) (2000) 1734–1736.
[36] D.J. Mead, Free wave propagation in periodically supported, infinite beams, J. Sound Vib. 11 (2) (1970) 181–197.
[37] G.H. Koo, Y.S. Park, Vibration reduction by using periodic supports in a piping system, J. Sound Vib. 210 (1) (1998) 53–68.
[38] D. Yu, Y. Liu, G. Wang, L. Cai, J. Qiu, Low frequency torsional vibration gaps in the shaft with locally resonant structures, Phys. Lett. 348 (3–6) (2006) 410–415.
[39] D. Yu, Y. Liu, G. Wang, H. Zhao, J. Qiu, Flexural vibration band gaps in Timoshenko beams with locally resonant structures, J. Appl. Phys. 100 (12) (2006), 124901.
[40] D. Yu, Y. Liu, H. Zhao, G. Wang, J. Qiu, Flexural vibration band gaps in Euler-Bernoulli beams with locally resonant structures with two degrees of freedom, Phys. Rev. B 73 (6) (2006), 064301.
[41] D. Yu, J. Wen, H. Zhao, Y. Liu, X. Wen, Vibration reduction by using the idea of phononic crystals in a pipe-conveying fluid, J. Sound Vib. 318 (1–2) (2008) 193–205.
[42] D. Yu, J. Wen, H. Shen, X. Wen, Propagation of steady-state vibration in periodic pipes conveying fluid on elastic foundations with external moving loads, Phys. Lett. 376 (45) (2012) 3417–3422.
[43] D. Yu, J. Wen, H. Shen, Y. Xiao, X. Wen, Propagation of flexural wave in periodic beam on elastic foundations, Phys. Lett. 376 (4) (2012) 626–630.
[44] Y. Xiao, J. Wen, D. Yu, X. Wen, Flexural wave propagation in beams with periodically attached vibration absorbers: band-gap behavior and band formation mechanisms, J. Sound Vib. 332 (4) (2013) 867–893.
[45] J-h Wu, H-z Zhu, Y-d Sun, Z-y Yin, M-z Su, Reduction of flexural vibration of a fluid-filled pipe with attached vibration absorbers, Int. J. Pres. Ves. Pip. 194 (2021), 104525.
[46] J. Wu, H. Zhu, Z. Yin, Y. Sun, Vibration wave propagation analysis of a liquid-filled pipe–plate coupled system with multiple supports, AIP Adv. 11 (2) (2021), 025110.
[47] W. Ji, W. Sun, D. Wang, Z. Liu, Optimization of aero-engine pipeline for avoiding vibration based on length adjustment of straight-line segment, Front Mech Eng Prc 17 (1) (2022) 11.
[48] M. Anklin, W. Drahm, A. Rieder, Coriolis mass flowmeters: Overview of the current state of the art and latest research, Flow Meas. Instrum. 17 (6) (2006) 317–323.
[49] A.K. Kohli, B.C. Nakra, Vibration analysis of straight and curved tubes conveying fluid by means of straight beam finite elements, J. Sound Vib. 93 (2) (1984) 307–311.